

Constraining twin stars with cold neutron star cooling data

Melissa Mendes*

*McGill University, Department of Physics and Trottier Space Institute at McGill, H3A2T8 Montreal, Canada,
Technische Universität Darmstadt, Department of Physics, 64289 Darmstadt, Germany,
ExtreMe Matter Institute EMMI, GSI Helmholtzzentrum für Schwerionenforschung GmbH, 64291 Darmstadt, Germany,
Max-Planck-Institut für Kernphysik, Saupfercheckweg 1, 69117 Heidelberg, Germany*

Jan-Erik Christian†

Hamburger Sternwarte, University of Hamburg, Gojenbergsweg 112, 21029 Hamburg, Germany

Farrukh J. Fattoyev‡

Department of Mathematics and Physics, Manhattan College, Riverdale, NY 10471, USA

Jürgen Schaffner-Bielich

*Institut für Theoretische Physik, Goethe Universität,
Max von Laue-Str. 1, D-60438 Frankfurt am Main, Germany*

(Dated: August 13, 2024)

We investigate the influence of a phase transition from hadronic matter to a deconfined quark phase inside a neutron star on its cooling behaviour. We take particular care that all equations of state under investigation are compatible with astrophysical constraints as well as are able to reproduce finite nuclear properties. We find that while the inferred neutrino luminosity of cold transiently-accreting star MXB 1659-29 is reproduced in all of the constructed twin star models, the luminosity of colder source SAX J1808.4-3658 cannot be described by equations of state with quark-hadron transition densities below 1.7 saturation density, suggesting that twin stars with such low density transitions to the quark phase are not realized in nature. We also discuss how constraints to the quark-hadron phase transition density are strongly dependent on the cooling effectiveness of quark phase reactions.

Keywords: quark-hadron phase transition, neutron star cooling, twin stars

I. INTRODUCTION

The unique high-density regime of neutron stars has long been established as an ideal laboratory for the investigation of nuclear bulk matter properties, specifically the equation of state (EOS). Nonetheless, there are great technical difficulties in both theoretically determining the EOS by performing a first-principles calculation from QCD, and experimentally constraining the EOS with nuclear or astrophysical measurements.

Currently, the low-density region of equations of state, up to at least saturation density, n_{sat} , can be constrained with experimentally determined ground state properties of finite nuclei, such as binding energy per nucleon, charge radii and neutron skin thickness (see, for example, [1–4]). A viable way to construct an equation of state able to reproduce these properties is the relativistic mean field (RMF) approach [5–13]. It generates EOSs that are highly parameterized by the strengths of various meson interactions, which are sensitive to different baryon densities of the EOS. In addition, its EOSs are covariant, so when extrapolated to the neutron-star regime, causality

is naturally preserved, thus, this technique is particularly suited for the incorporation of the known nuclear experimental constraints, at densities below and around saturation density, and observational astrophysical constraints, at larger densities. The high-density neutron star EOS constraints include heavy ion collision experiments [14–16] and neutron stars’ observables such as maximum mass [17–21], tidal deformability [22, 23] and radius measurements. The NICER telescope in special has provided particularly constraining simultaneous measurements of mass and radius of selected pulsars [24–27], setting strong constraints to the equation of state [28–31]. However, by combining all these measurements, one notices that there is an apparent tension between neutron star masses, which reach at least values of $2 M_{\odot}$ [17–20], therefore requiring a stiff equation of state, and the tidal deformability (Λ) reported for GW170817, which suggests a soft equation of state [23]. Nonetheless, equations of state usually considered too stiff to reproduce the tidal deformability constraint can be brought into agreement with it if a quark-hadron phase transition is present [32–36]. This phase transition generates the so-called hybrid stars, formed by an inner quark core with nucleonic outer core and crust [37–44], which feature smaller values of tidal deformability, more in line with naturally soft EOSs.

A subcategory of hybrid stars with some significance are twin stars, which are two stars with the same mass

* melissa.mendes@physik.tu-darmstadt.de

† jan-erik.christian@uni-hamburg.de

‡ ffattoyev01@manhattan.edu

and different radii. Such configurations can only be generated by an EOS with a strong phase transition or a rapid cross-over[45–53]. Thus, observing twin stars would be a smoking gun signal for the presence of a transition to a new phase in the core of at least some neutron stars. In this context, it is interesting to investigate whether cooling data could further constrain the existence of twin stars or set limits on the density in which such a phase transition would take place.

Previous studies have investigated the cooling behavior of quark-hadron hybrid stars with different EOSs [54, 55], suggesting that they are able to reproduce current stars’ temperature evolution data. Another study [56] has performed estimates on the effectiveness of quark dUrca cooling reactions in hybrid stars that are consistent with cold stars’ luminosities, but they lacked a consistent EOS for the quark phase. To our knowledge, the present work is the first study focusing on twin stars without strangeness in the hadronic phase, particularly the ones able to reproduce all other current astrophysical observations. Furthermore, we focus on very cold transiently-accreting neutron stars, whose low temperatures strongly indicate the presence of fast-cooling processes in the stars’ core [57]. Reproducing the inferred neutrino luminosity of cold sources can set an upper limit on the star core volume submitted to fast-cooling processes, thus potentially constrain the quark-hadron phase transition density, particularly for EOSs with direct Urca (dUrca) neutrino emission reactions in the quark phase only.

In section II, we describe the nucleonic and quark EOSs

used in this investigation, as well as the calculation of dUrca emissivities and the estimation of the neutrino luminosity of the sources. These luminosities are reproduced in section III, where we also show the predicted hybrid star masses of each source as a function of the quark-hadron phase transition density. The relationship between the EOSs parameters and the reproduction of neutron stars’ luminosities is expanded in section IV.

II. THEORETICAL FRAMEWORK

A. Equation of state

For the nucleonic equation of state we employ a relativistic mean field approach [5–13] making use of the parameterizability in this ansatz. The equation of state can be expanded as

$$E(n, \alpha) = E(n, 0) + E_{\text{sym}}(n)\alpha^2 + \dots \quad (1)$$

where $E(n, 0)$ is the energy per nucleon of symmetric matter, $\alpha = 1 - 2y$ is the asymmetry parameter with $y = n_p/(n_N + n_p)$, where n_x is the neutron’s or proton’s number density and $E_{\text{sym}}(n)$ is the symmetry energy, which quantifies the energy difference between symmetric nuclear matter and pure neutron matter.

To provide a detailed understanding of the EOS in the context of the RMF theory, we first discuss the Lagrangian density given by $\mathcal{L} = \mathcal{L}_0 + \mathcal{L}_{\text{int}}$, where the first term is the free Lagrangian density, in natural units,

$$\mathcal{L}_0 = \bar{\psi} (i\gamma^\mu \partial_\mu - M) \psi + \frac{1}{2} (\partial_\mu \phi \partial^\mu \phi - m_s^2 \phi^2) + \frac{1}{2} m_v^2 V_\mu V^\mu - \frac{1}{4} F_{\mu\nu} F^{\mu\nu} + \frac{1}{2} m_\rho^2 \mathbf{b}_\mu \cdot \mathbf{b}^\mu - \frac{1}{4} V_{\mu\nu} V^{\mu\nu} - \frac{1}{4} \mathbf{b}_{\mu\nu} \cdot \mathbf{b}^{\mu\nu}, \quad (2)$$

and the second term is the interacting Lagrangian density,

$$\begin{aligned} \mathcal{L}_{\text{int}} = & \bar{\psi} \left[g_s \phi - \left(g_v V_\mu + \frac{g_\rho}{2} \boldsymbol{\tau} \cdot \mathbf{b}_\mu + \frac{e}{2} (1 + \tau_3) A_\mu \right) \gamma^\mu \right] \psi - \frac{\kappa}{3!} (g_s \phi)^3 - \frac{\lambda}{4!} (g_s \phi)^4 + \frac{\zeta}{4!} (g_v^2 V_\mu V^\mu)^2 + \\ & + \Lambda_v (g_v^2 V_\mu V^\mu) (g_\rho^2 \mathbf{b}_\mu \cdot \mathbf{b}^\mu), \end{aligned} \quad (3)$$

where

$$\begin{aligned} F_{\mu\nu} &= \partial_\mu A_\nu - \partial_\nu A_\mu, \\ V_{\mu\nu} &= \partial_\mu V_\nu - \partial_\nu V_\mu, \\ \mathbf{b}_{\mu\nu} &= \partial_\mu \mathbf{b}_\nu - \partial_\nu \mathbf{b}_\mu. \end{aligned} \quad (4)$$

In this Lagrangian, the nucleon interactions are modeled by exchanging photons, represented by the field A_μ , and various mesons. The field ϕ represents the interactions of the scalar-isoscalar σ -meson responsible for intermediate attractive interactions, V^μ represents the vector-isoscalar ω -meson responsible for short-range repulsive interactions and \mathbf{b}_μ represents the vector-isovector ρ -meson. The latter introduces isospin dependence in the interactions and is crucial for describing the differences

between protons and neutrons in nuclear matter [58]. In addition to meson-nucleon interactions, the Lagrangian density includes scalar and vector self-interactions. In particular, the ω -meson self-interactions, as described by the parameter ζ , soften the equation of state at high density and can be tuned to reproduce the maximum mass of a neutron star [10]. Hence, we use ζ as one of our free parameters ranging between $0.00 \leq \zeta \leq 0.02$ to make sure the EOSs are consistent with the latest observations [17, 18, 20].

The symmetry energy can be expanded around saturation density,

$$E_{\text{sym}}(n) = J + Lx + \frac{1}{2} K_{\text{sym}} x^2 + \dots, \quad (5)$$

with the expansion parameter $x = (n - n_{\text{sat}})/3$. J , L and K_{sym} are, respectively, the value, slope and curvature of the symmetry energy at saturation. These coefficients can be constrained by nuclear experiments, however, there are conflicting constraints on the density slope of the symmetry energy L (see, for example [59] and references within). While the measurement of electric dipole polarizability suggests a soft value of $L = 47 \pm 8$ MeV [60] in agreement with the CREX result of the neutron skin measurement of Ca^{48} [2], the PREX measurements of the neutron skin in Pb^{208} [61] prefer a stiffer value for the slope of the symmetry energy, of $L = 106 \pm 37$ MeV. A broader range of estimations for the slope parameter L from neutron skin experiments place it between either $L = 40 - 60$ MeV [2–4] or much higher $L = 121 \pm 47$ MeV [1, 3, 4]. To cover a broad range of the slope parameter L consistent with these experimental constraints, we use EOSs with $L = 50$ MeV and $L = 90$ MeV.

Additionally, we take the Dirac effective mass, $M^* = M - g_s \phi$, as our third free parameter, where M is the nucleon mass. This parameter affects the pressure of symmetric nuclear matter at intermediate densities [62], and for an optimal parametrization of the relativistic mean-field model, $m^* = M^*/M$ should be in the range of $0.55 \lesssim m^* \lesssim 0.65$, [63, 64], although larger values of m^* , up to 0.75 may also be allowed [65]. We use two values of m^* in the EOSs, of 0.55 and 0.60. Thus, we have three parameters that control the density dependence of the EOS at various densities: m^* , at intermediate densities, ζ , at high densities, and L , around saturation for the nuclear symmetry energy. We combine those parameters within 4 EOSs: $L = 50$ MeV, $m^* = 0.60$, $\zeta = 0$ (EOS I); $L = 50$ MeV, $m^* = 0.60$, $\zeta = 0.02$ (EOS II); $L = 90$ MeV, $m^* = 0.55$, $\zeta = 0.02$ (EOS III) and $L = 90$ MeV, $m^* = 0.60$, $\zeta = 0.02$ (EOS IV). Comparing the results from each of them in pairs, one can check the effect of a given parameter on hybrid star cooling.

In particular, an important quantity to examine regarding cooling is the direct Urca threshold, which refers to the proton fraction $Y_p = Z/A$ in neutron star matter above which direct Urca reactions are allowed by energy-momentum conservation. In the simplest case, when muons are not present in the EOS, the dUrca threshold is found to be $Y_{p,\text{dUrca}} = 1/9$, but in more realistic EOSs including muons, it can be found by solving the charge neutrality and momentum conservation equations that lead to the following dynamical equation [58],

$$\left(\frac{1 - Y_p}{Y_p}\right)^{1/3} = 1 + (1 - \mathcal{Y})^{1/3}, \quad (6)$$

where $\mathcal{Y} = Z_\mu/Z$ is the muon charge fraction. Therefore, the dUrca threshold is strongly dependent on the equation of state and it has been shown [66, 67] that EOSs with larger L have a lower dUrca threshold density. This trend can be understood by observing that larger L EOSs have larger symmetry energy at high densities, which makes the neutron star matter more symmetric and allows the proton fraction to more easily exceed the

TABLE I. Slope of symmetry energy (L (MeV)), Dirac effective mass (m^*), ω -meson self-interactions (ζ), dUrca threshold proton fraction ($Y_{p,\text{dUrca}}$), dUrca threshold density (n_{dUrca}), dUrca threshold mass ($m_{\text{dUrca}}(M_\odot)$) and maximum mass ($m_{\text{max}}(M_\odot)$) for EOS I, EOS II, EOS III and EOS IV.

	L	m^*	ζ	$Y_{p,\text{dUrca}}$	n_{dUrca}	m_{dUrca}	m_{max}
EOS I	50	0.60	0.0	0.1375	3.51	2.58	2.70
EOS II	50	0.60	0.02	0.1376	3.55	1.87	2.09
EOS III	90	0.55	0.02	0.1319	1.77	1.01	2.19
EOS IV	90	0.60	0.02	0.1321	1.78	0.92	2.11

required threshold at lower densities. In other words, Y_p is directly proportional to L , according to the relation

$$Y_p \simeq \frac{64}{3\pi^2 n_{\text{sat}}} \left(\frac{J + Lx + \frac{1}{2}K_{\text{sym}}x^2 + \dots}{\hbar c} \right)^3, \quad (7)$$

for matter in beta equilibrium. Increasing the slope of symmetry energy L , independently of the other expansion parameters, directly increases the proton fraction, thus reducing the density at which the dUrca threshold Y_p is reached. There is no one-to-one correspondence between the remaining parameters m^* and ζ and the expansion parameters in Eq. 7, so a simple relation between the dUrca threshold and m^* or ζ cannot be constructed. Nonetheless, EOSs with larger m^* or ζ present slightly increased dUrca threshold densities, as seen in table I, but the influence of those quantities in hybrid star cooling is more clearly seen in the dUrca emissivity rather than the dUrca threshold.

To build quark-hadron phase transitions in the nucleonic EOSs, we assume that at a sufficiently high pressure, p_{trans} , the nucleonic equation of state is replaced by a quark phase. We model this by using a Maxwell construction, meaning that the phase transition is realized as a discontinuity in energy density at a constant pressure of p_{trans} . The quark phase is described using a constant speed of sound equation of state. This ansatz has been well established [49, 68] and takes the following mathematical form:

$$\epsilon(p) = \begin{cases} \epsilon_{\text{RMF}}(p) & p < p_{\text{trans}} \\ \epsilon_{\text{trans}} + \Delta\epsilon + c_{\text{QM}}^{-2}(p - p_{\text{trans}}) & p > p_{\text{trans}}, \end{cases} \quad (8)$$

in geometric units, where $c = 1$ and c_{QM} is the constant sound speed of the quark phase. The transitional pressure p_{trans} and the jump in energy density $\Delta\epsilon$ are free parameters. The transition pressure can be used interchangeably with the energy density at the point of transition ϵ_{trans} in the nucleonic phase, through the connection $\epsilon_{\text{trans}} = \epsilon_{\text{RMF}}(p_{\text{trans}})$.

Following the works of [33, 53, 69], we build quark-hadron phase transitions that generate twin stars. This criterium is a strong constraint mostly for EOS II, forbidding phase transitions between $2.3 \leq n \leq 4n_{\text{sat}}$ for that equation of state. Thus, hybrid stars in this density region are not investigated in this work, even though

TABLE II. Parameters of the hybrid EOS built with nucleonic EOS I (upper left), EOS II (upper right), EOS III (lower left) and EOS IV (lower right). Transition density (n_{trans}) given in terms of saturation density (n_{sat}), transition pressure (p_{trans}) and energy density jump ($\Delta\epsilon$) given in MeV/fm³. The cases where nucleonic dUrca processes are allowed are marked with a star.

EOS I	EOS II
$n_{\text{trans}} = 1, p_{\text{trans}} = 3, \Delta\epsilon = 170,$	$n_{\text{trans}} = 1.2, p_{\text{trans}} = 5, \Delta\epsilon = 180$
$n_{\text{trans}} = 1.29, p_{\text{trans}} = 6, \Delta\epsilon = 260,$	$n_{\text{trans}} = 1.87, p_{\text{trans}} = 20, \Delta\epsilon = 223$
$n_{\text{trans}} = 1.84, p_{\text{trans}} = 25, \Delta\epsilon = 220,$	$n_{\text{trans}} = 2.2, p_{\text{trans}} = 35, \Delta\epsilon = 241$
$n_{\text{trans}} = 2, p_{\text{trans}} = 38, \Delta\epsilon = 236,$	$n_{\text{trans}}^* = 4, p_{\text{trans}} = 153, \Delta\epsilon = 250$
$n_{\text{trans}} = 2, p_{\text{trans}} = 38, \Delta\epsilon = 280$	$n_{\text{trans}}^* = 4.07, p_{\text{trans}} = 160, \Delta\epsilon = 245$
	$n_{\text{trans}}^* = 4.3, p_{\text{trans}} = 180, \Delta\epsilon = 229$
	$n_{\text{trans}}^* = 4.6, p_{\text{trans}} = 205, \Delta\epsilon = 200$
EOS III	EOS IV
$n_{\text{trans}} = 1, p_{\text{trans}} = 4, \Delta\epsilon = 130,$	$n_{\text{trans}} = 0.9, p_{\text{trans}} = 3.2, \Delta\epsilon = 132$
$n_{\text{trans}} = 1.5, p_{\text{trans}} = 12, \Delta\epsilon = 172,$	$n_{\text{trans}} = 1.28, p_{\text{trans}} = 7, \Delta\epsilon = 285$
$n_{\text{trans}}^* = 2, p_{\text{trans}} = 27, \Delta\epsilon = 206,$	$n_{\text{trans}} = 1.67, p_{\text{trans}} = 15, \Delta\epsilon = 182$
$n_{\text{trans}}^* = 2.18, p_{\text{trans}} = 36, \Delta\epsilon = 220$	$n_{\text{trans}}^* = 1.93, p_{\text{trans}} = 23, \Delta\epsilon = 211$
$n_{\text{trans}}^* = 2.2, p_{\text{trans}} = 38, \Delta\epsilon = 296$	$n_{\text{trans}}^* = 2.16, p_{\text{trans}} = 32, \Delta\epsilon = 226$
	$n_{\text{trans}}^* = 2.37, p_{\text{trans}} = 42, \Delta\epsilon = 255$

they could be compatible with observational data. We vary the phase transition parameters p_{trans} and $\Delta\epsilon$ to allow for the smallest and largest possible n_{trans} generating twin stars that fit the astrophysical constraints. Different combinations of the parameters L and ζ affect the stiffness of the nucleonic part of the EOSs, which restricts the quark phase transitions resulting in hybrid stars compatible with astrophysical data constraints. In particular, EOSs with larger ζ accommodate larger quark phase transition densities, but the tidal deformability observation restricts EOSs with larger L -value to relatively low-density phase transitions, around $2 n_{\text{sat}}$. The parameters of all phase transitions built in this work are shown in table II.

Finally, we combine the quark-hadron hybrid core equation of state with the Baym-Pethick-Sutherland EOS [70] for the outer crust and the Negele-Vautherin EOS [71] for the inner crust. Using other crust equations of state would not significantly change the calculated masses, even if it may slightly alter radii predictions [72]. While solving the TOV equations, we have often observed the presence of a single stable hybrid star in the first mass-radius branch, even when usual stability criteria, like the so-called Seidov limit [73], would suggest otherwise. This phenomenon is a function of the step-size radius used in solving the TOV equations and it has been observed before, but not documented [74]. It does not affect the calculations performed in this work.

B. Hybrid star cooling

The neutron stars under study have high inferred neutrino luminosities, thus we focus on neutrino emitting fast-cooling processes, which take place at the neutron star core, and ignore slow-cooling, as well as crust-cooling processes, because their cooling rates are subdominant

in cold neutron stars [75]. The determination of neutron stars surface temperature and envelope composition in this simplified scenario is discussed in section II C.

For the equations of state used in this work, the relevant reactions are nucleonic neutrino direct Urca reactions for the nucleonic part of the EOS, $n \rightarrow p + l + \bar{\nu}_l$ and $p + l \rightarrow n + \nu_l$, where l stands for leptons, and quark direct Urca reactions for the quark part of the EOS, $d \rightarrow u + e^- + \bar{\nu}_e$ and $u + e^- \rightarrow d + \nu_e$, with corresponding neutrino emissivities, respectively derived in [75] and [76],

$$\epsilon_{\text{Urca}} = \frac{457\pi}{10080} G_{\text{F}}^2 \cos^2 \theta_{\text{C}} (1 + 3g_{\text{A}}^{*2}) m_{\text{n}}^{L*} m_{\text{p}}^{L*} \times \frac{(3\pi^2 Y_{\text{e}} n)^{1/3}}{\hbar^9 c^4} (k_{\text{B}} T)^6 \quad (9)$$

$$\epsilon_{\text{q Urca}} = \frac{914}{315} \frac{G_{\text{F}}^2 \cos^2 \theta_{\text{C}}}{\hbar^7 c^6} (3Y_{\text{e}})^{1/3} \alpha \pi^2 n (k_{\text{B}} T)^6. \quad (10)$$

Corrections due to in-medium interactions are included in the effective Landau masses $m_{\text{n}}^{L*}, m_{\text{p}}^{L*}$, given by $m_i^{L*} = \sqrt{(M_i^*)^2 + (\hbar k_{\text{F}i}/c)^2}$ with M_i^* being the Dirac effective mass. Here $g_{\text{A}}^* \simeq g_{\text{A}} \left(1 - \frac{n}{4.15(n_{\text{sat}} + n)}\right)$ is the axial vector coupling that depends on the baryon density [77], G_{F} is the weak interaction constant, k_{B} is the Boltzmann constant, α is the strong coupling constant and θ_{C} is the Cabibbo angle.

Considering up and down quarks cooling processes only, we fix the electron fraction in the quark phase to $Y_{\text{e}} = 10^{-5}$ and the strong coupling constant $\alpha = 0.12$, unchanging with density. The effect of these approximations on the estimated masses of the sources and phase transition density is discussed in section IV. The quark EOS we use is agnostic about the presence of strange

quarks in the quark phase, but for simplicity we assume they do not participate in the cooling reactions here. Possible color superconducting phases are also ignored for the same reason.

Given the nature of first-order transitions, no quark-hadron mixed phase is present for a Maxwell construction in neutron stars. Therefore, if the phase transition happens before the nucleonic dUrca threshold is reached, quark dUrca processes will be the only fast-cooling neutrino reactions of the hybrid star. These cases are indicated by star symbols (*) in table II.

Some gap models describing superfluidity and superconductivity in the nucleonic core are included, following the parametrization originally described in [78]:

$$\Delta(k_{Fx}) = \Delta_0 \frac{(k_{Fx} - k_0)^2}{(k_{Fx} - k_0)^2 + k_1} \frac{(k_{Fx} - k_2)^2}{(k_{Fx} - k_2)^2 + k_3}, \quad (11)$$

where k_{Fx} is the Fermi momentum of the nucleons x and the quantities Δ_0 , k_0 , k_1 , k_2 and k_3 are free parameters. We work with combinations of neutron triplet superfluid gap models NT SYHHP [79], NT AO [80], NT EEHO [81] and proton singlet superconducting gap models PS CCDK [82] and PS BCLL [83], which form a representative sample of nuclear pairing models, including examples where both most and very few of the nucleons in the core are paired.

C. Transiently-accreting neutron stars envelope and temperature

We reproduce the inferred neutrino luminosity of two transiently-accreting neutron stars in low-mass X-ray binaries: MXB 1659-29 and SAX J1808.4-3658. These sources were chosen for their low luminosity, which suggests that fast-cooling processes must be active in their core [57]. In particular, SAX J1808.4-3658 is one of the coldest neutron stars ever observed, thus its cooling pattern might strongly constrain the core EOS. MXB 1659-29 was selected because three cycles of accretion-quiescence have been observed for this source, which has improved the accuracy of its crust heat transport models and temperature estimation, allowing for a more precise determination of its neutrino luminosity [56, 84].

The estimated temperature of MXB 1659-29 as measured by an observer at infinity, T_e^∞ , is taken from [84, 85] to be 55 eV. We also assume for this source an envelope composition of mainly light elements, following their detailed modelling of crust cooling, consistent with the latest data [86]. The inferred neutrino luminosity of MXB 1659-29 is estimated from the amount of deposited energy from accretion, considering its inferred average mass accretion rate $\langle \dot{M} \rangle \approx 1.5 \times 10^{-9} M_\odot/\text{yr}$ [87], following the procedure described in [88], which leads to an expected value of neutrino luminosity observed at infinity $L_\nu = (3.91 \pm 2) \times 10^{34}$ erg/s, 1σ standard deviation. The major sources of uncertainty to this neutrino luminosity

estimation are the estimated source's distance and envelope composition. Other possible sources of uncertainty in the crust cooling modelling, such as the uniformity of the outburst accretion rate, were proven not to impact the neutrino luminosity estimation [84]. Detailed models for the crust cooling of SAX J1808.4-3658 are not available, thus, we work with an estimated upper limit to its neutrino luminosity of $L_\nu = 1 \times 10^{32} - 1 \times 10^{33}$ erg/s, obtained considering its average accreted mass $\langle \dot{M} \rangle = 9 \times 10^{-12} M_\odot/\text{yr}$ [89], such that the approximate neutrino luminosity is the mass accretion rate times the energy released by crust reactions, $Q \approx 0.5 - 2$ MeV/nucleon mass. We take $T_e^\infty = 36_{-8}^{+4}$ eV for this source [89], and make no assumptions on its envelope composition.

III. RESULTS

In this section, we calculate the range of neutron star masses corresponding to the estimated lower and upper limits of neutrino luminosity for each source. This provides a check to the feasibility of the phase transitions built and allows us to better understand the effects of twin stars in the luminosity curves. Since core collapse supernova simulations suggest that neutron stars lighter than $\approx 1 M_\odot$ are not formed [90–94], we do not include such stars in our analysis, but still display them in some plots for easier visualization.

A. Hybrid stars with nucleonic $L50$ EOS

Depending on the equation of state, nucleonic superfluidity model and the onset of the quark phase, the inferred neutrino luminosities of MXB 1659-29 and SAX J1808.4-3658 can be reached with quark dUrca processes alone, nucleonic dUrca processes alone or a combination of them. For EOS I, all quark phase transitions take place before the onset of the dUrca threshold, thus the neutrino luminosities of cold sources are reached with quark dUrca processes only. Increasing the value of the ζ parameter to 0.02 (EOS II) considerably softens the EOS and allows for larger phase transition densities. In that case, all hybrid stars with phase transition densities smaller than the dUrca threshold, $3.55 n_{\text{sat}}$, cool predominantly through quark dUrca processes, while the ones with larger phase transition densities cool mainly through nucleonic dUrca processes.

Figure 1 displays the predicted hybrid star masses for MXB 1659-29, considering also nuclear pairing in the nucleonic phase for EOS II stars. The data points in blue correspond to EOS I with a phase transition at $n_{\text{trans}} = 2 n_{\text{sat}}$, but $\Delta\epsilon = 280$ MeV, to differentiate it from the point in black with phase transition at $n_{\text{trans}} = 2 n_{\text{sat}}$ and $\Delta\epsilon = 236$ MeV. Increasing the $\Delta\epsilon$ while keeping the other phase transition parameters unaltered slightly reduces the mass range, but the most important predictor

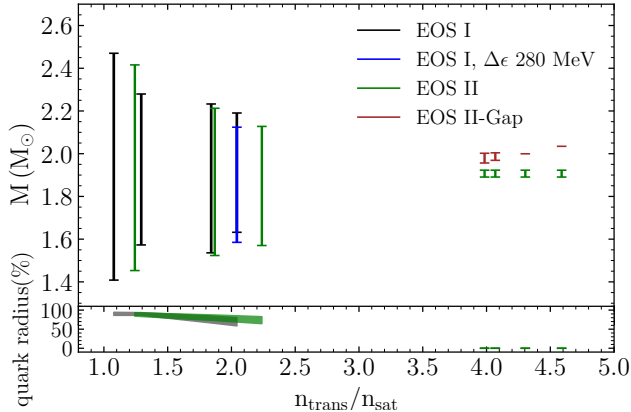


FIG. 1. Total masses of the hybrid stars with MXB 1659-29’s lower and upper inferred neutrino luminosities, built with nucleonic EOS I (in black) and EOS II (in green). The density transitions $n_{\text{trans}}/n_{\text{sat}}$ are represented in the x-axis. The blue line marks the special case of EOS I, $p_{\text{trans}} = 38$ MeV, $n_{\text{trans}} = 2 n_{\text{sat}}$, $\Delta\epsilon = 280$ MeV to differentiate it from $\Delta\epsilon = 236$ MeV with same transition density, in black. In brown, the results for EOS II with nuclear pairing combination NT AO+PS CCYps are shown. In the lower plot, the hybrid stars corresponding quark radius fraction in relation to total radius is shown.

of mass range size is still the transition density n_{trans} , that determines the quark volume fraction in the hybrid star. For EOS II, the gap model combination NT AO+PS CCYps, shown in Figure 1, provides a strong dUrca suppression, resulting in a large difference to the non-paired case, which eventually fails to reproduce the lower luminosity limit of source MXB 1659-29 for large phase transition densities, $n_{\text{trans}} \geq 4.3 n_{\text{sat}}$. That is an example situation where including nuclear pairing in the nucleonic phase does not necessarily increase the calculated mass range, because then, the quark dUrca cooling again becomes dominant and the decisive factor becomes the quark volume, which might not be large enough to reproduce a source’s luminosity. This situation is particularly clear for combinations of strong superfluidity and superconductivity gap models such as PS AO+NT SYHHP or PS CCDK+NT AO.

For both EOS, the mass ranges predicted for hybrid stars with early phase transitions ($n_{\text{trans}} \lesssim 2 n_{\text{sat}}$) in Figure 1 are larger because these stars have a larger quark phase volume fraction (close to 100%), thus present a larger volume under quark dUrca cooling. This suggests that, for those EOS and phase transitions, the full range of inferred luminosities of colder sources is potentially not achieved in the quark volume available, that is, these twin stars would not reproduce the neutrino luminosity of colder sources. This is indeed the case for EOS I and EOS II, which fail to completely reproduce SAX J1808.4-3658’s inferred luminosity (between 10^{32} to 10^{33} erg/s) for phase transitions with $n_{\text{trans}} < 1.8 n_{\text{sat}}$, for all

envelope compositions tested. This scenario is examined in more detail in Figure 2 and Figure 3. In Figure 2, the calculated masses for SAX J1808.4-3658 are shown, considering a light element envelope and $28 \leq T^\infty \leq 40$ eV. The predicted masses for each temperature are indicated with different symbols. Despite the general trend of lower effective temperatures resulting in larger masses for SAX J1808.4-3658, the fraction of quark radius necessary to reach the inferred luminosity is always between 90% and 100% for $n_{\text{trans}} < 1.8 n_{\text{sat}}$. In Figure 3, we examine in more detail the luminosity curves of EOS I with $T^\infty = 36$ eV, where the inferred luminosity of SAX J1808.4-3658 is indicated by the horizontal grey band and the first stable star for each phase transition is represented by a dot, such that lower masses correspond to unstable stars. Hence, it is clear that the lower limit of SAX J1808.4-3658’s luminosities is reached only in unstable stars for phase transitions $n_{\text{trans}} < 1.8 n_{\text{sat}}$, with light element envelope, thus these phase transitions are inconsistent with the full error band of cooling data.

Including nuclear pairing in EOS II with SAX J1808.4-3658’s effective temperatures produces a similar effect to that seen in Figure 1, for MXB 1659-29. Strong pairing such as NT AO+PS CCYps reduces the predicted mass range because it suppresses the nucleonic dUrca reactions, forcing most of the luminosity to be generated by quark dUrca processes. In this scenario, lower temperatures particularly struggle to reproduce the lower limit of SAX J1808.4-3658’s luminosity. We also notice that, for both EOS, assuming a heavy element envelope composition for SAX J1808.4-3658 results in luminosities inconsistent with the source’s inferred cooling data for most phase transitions and temperatures.

B. Hybrid stars with nucleonic $L90$ EOS

The dUrca threshold of nucleonic $L90$ EOS is lower than the $L50$ EOS (see table I), thus more of the phase transitions built involve both nucleonic and quark dUrca cooling. However, their increased stiffness only allows for relatively low density phase transitions, of at most $n_{\text{trans}} \lesssim 2.4 n_{\text{sat}}$, to be compatible with astrophysical data [36, 69, 95], hence only a relatively small range of possible phase transition densities can be probed. The different Dirac M^* of EOS III and EOS IV only marginally affect the allowed quark-hadron phase transition densities and luminosity curves.

The general pattern of larger mass ranges for lower phase transition densities is repeated, as seen in Figure 4 and 5. For these EOS, large quark volumes are still needed to reproduce the upper limit of inferred luminosities for MXB 1659-29, thus colder sources tend to be incompatible with small phase transition densities, around $n_{\text{trans}} < 1.8 n_{\text{sat}}$. This feature is observed when reproducing SAX J1808.4-3658’s data, whose full inferred luminosity band is only achieved assuming a light element envelope composition and $n_{\text{trans}} \gtrsim 1.9 n_{\text{sat}}$,

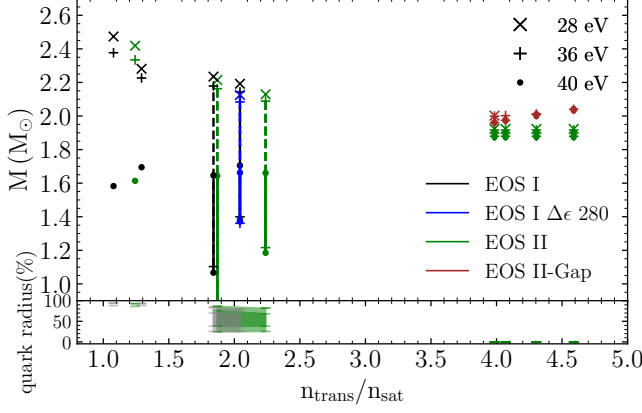


FIG. 2. Total masses of the hybrid stars with SAX J1808.4-3658's lower and upper inferred neutrino luminosities, built with nucleonic EOS I (in black) and EOS II (in green), for $T^\infty = 28$ eV (crosses and dotted lines), $T^\infty = 36$ eV (plus signs and dashed lines) and $T^\infty = 40$ eV (circles and solid lines), with light element envelope. The blue line marks the special case of EOS I, $p_{\text{trans}} = 38$ MeV, $n_{\text{trans}} = 2 n_{\text{sat}}$, $\Delta\epsilon = 280$ MeV. In brown, the results for EOS II with nuclear pairing combination NT AO+PS CCYps are shown. In the lower plot, the hybrid stars corresponding quark radius fraction in relation to total radius is shown.

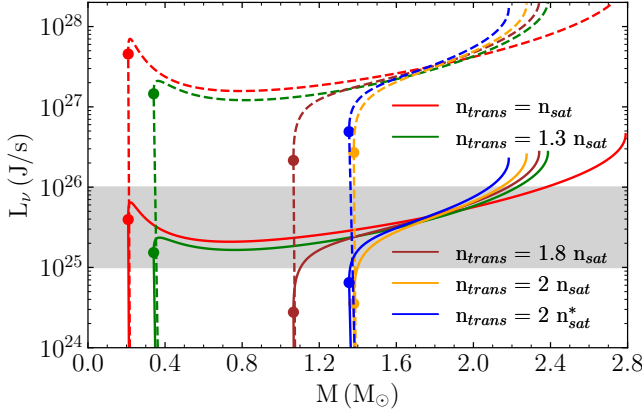


FIG. 3. Total luminosity and mass of EOS I hybrid stars for $T^\infty = 36$ eV with light elements envelope (solid lines) and heavy elements envelope (dashed lines). SAX J1808.4-3658 predicted luminosity is highlighted by the grey region. Different phase transitions are indicated by different colors according to the label. Circles mark the first stable star for each EOS. The blue line with label $n_{\text{trans}} = 2 n_{\text{sat}}^*$ is the case $p_{\text{trans}} = 38$ MeV, $n_{\text{trans}} = 2 n_{\text{sat}}$ and $\Delta\epsilon = 280$ MeV.

for both EOS III and IV and $28 < T^\infty \leq 40$ eV. A less likely but still possible scenario for this source is a heavy element envelope composition with $T^\infty = 28$ eV and $n_{\text{trans}} \gtrsim 1.9 n_{\text{sat}}$, where the luminosities are reached by nucleonic dUrca, thus the mass ranges are very small, or a light element envelope with $T^\infty = 36$ eV

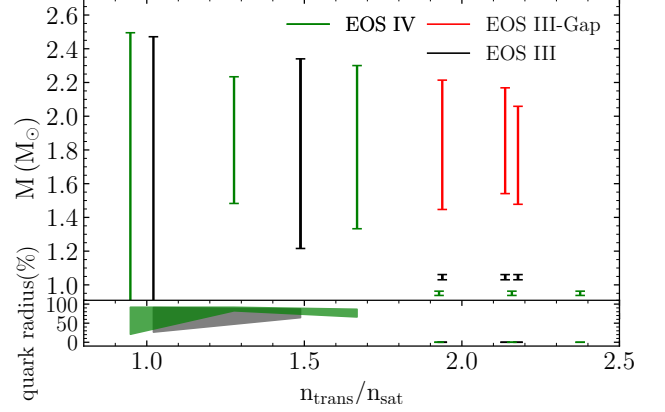


FIG. 4. Total masses of the hybrid stars with MXB 1659-29's lower and upper inferred neutrino luminosities, including superfluidity in nucleonic EOS III (PS CCDK+NT EEHOr gap model combination in red), without superfluidity (black), and nucleonic EOS IV without superfluidity (green). The density transitions $n_{\text{trans}}(n_{\text{sat}})$ are represented in the x-axis. In the lower plot, the hybrid stars corresponding quark radius fraction in relation to total radius is shown.

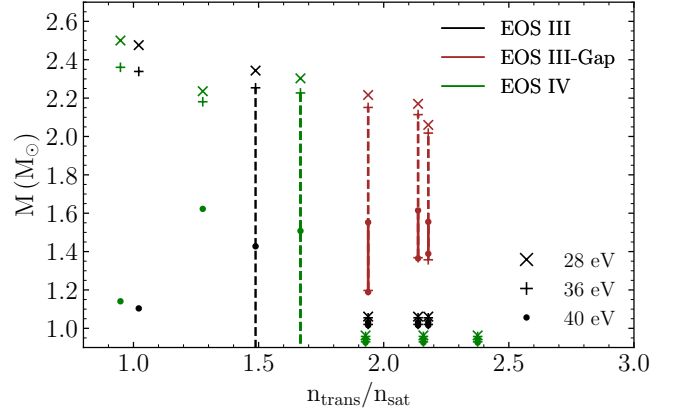


FIG. 5. Total masses of the hybrid stars with SAX J1808.4-3658's lower and upper inferred neutrino luminosities, including superfluidity in nucleonic EOS III (PS CCYps+NT AO gap model combination in brown), without superfluidity (black), and nucleonic EOS IV without superfluidity (green), for $T^\infty = 28$ eV (crosses and dotted-dashed lines), $T^\infty = 36$ eV (plus signs and dashed lines) and $T^\infty = 40$ eV (circles and solid lines), with light element envelope. The density transitions $n_{\text{trans}}(n_{\text{sat}})$ are represented in the x-axis.

and $n_{\text{trans}} = 1.5 n_{\text{sat}}$ for EOS III or $n_{\text{trans}} = 1.7 n_{\text{sat}}$ for EOS IV, where the source luminosity is reached by quark dUrca processes only, as shown in Figure 5 for the light element envelope composition. However, in these cases, SAX J1808.4-3658's lower luminosity limit is reached for neutron stars with masses $M < M_\odot$.

Including nuclear pairing results in quark dUrca prop-

cesses being dominant for densities $n_{trans} > 1.9 n_{sat}$, which leads to a visible increasing of the mass ranges from around solar mass, for the non-superfluid case, to values centered around $1.8 M_{\odot}$ for MXB 1659-29 and nuclear pairing model PS CCDK+NT EEHor, as seen in Figure 4. For SAX J1808.4-3658, including nuclear pairing also significantly increases the mass ranges above solar mass for both EOS, as seen in Figure 5 for EOS III. Both EOS favour strong proton superconductivity gap models, such as PS CCDK and PS CCYps, and are agnostic about the neutron superfluidity ones, given the relatively low densities of the quark phase, that starts before the effects of the neutron pairing can be significantly reflected on the luminosity curves.

IV. DISCUSSION AND CONCLUSIONS

Reproducing the luminosity of fast cooling sources with twin stars is challenging. Firstly, one must build quark-hadron EOS consistent with astrophysical data, for which the biggest limiting factor is the tidal deformability constraint provided by GW170817 [23]. Since our nucleonic EOSs feature comparatively large radii with large values of Λ , a small transition density is needed to achieve compatibility with this constraint, thus the range of allowed phase transition densities for EOS III and IV, with $L = 90$ MeV, is limited to $n < 2.5 n_{sat}$ and for EOS I, with $L = 50$ MeV, to $n < 2 n_{sat}$. The quark-hadron phase transition density for EOS II can be as high as $4.6 n_{sat}$, but the requirement that mass-radius contours from NICER [26, 27] are reproduced leaves a gap between the allowed phase transition densities such that $1.2 n_{sat} \leq n_{trans} \leq 2.2 n_{sat}$ or $4 n_{sat} \leq n_{trans} \leq 4.6 n_{sat}$. This EOS allows for a larger range of transition densities generating twin stars, opening up the high density regime.

However, due to the smaller efficiency of quark dUrca processes compared to nucleonic dUrca processes, stable twin stars with low density phase transitions tend to struggle reproducing the low luminosities of cold neutron stars. In particular, quark-hadron phase transition densities below $1.7 n_{sat}$ in twin stars of all EOS under study fail to reproduce the full range of SAX J1808.4-3658's inferred luminosities, usually only succeeding to reproduce their upper limit. Therefore, these low density quark-hadron phase transitions, up to 1.7 saturation density, are disfavoured over the ones able to reproduce the full luminosity range, suggesting that twin stars with low density transitions to the quark phase are not realized in nature.

EOS with larger phase transition densities successfully reproduce SAX J1808.4-3658's luminosity, often with a light element envelope composition and $28 \leq T^{\infty} \leq 36$ eV. For phase transition densities above the nucleonic dUrca threshold, that luminosity is obtained with nucleonic processes only and the quark cooling contribution is very minor and hardly detectable. In these cases, in-

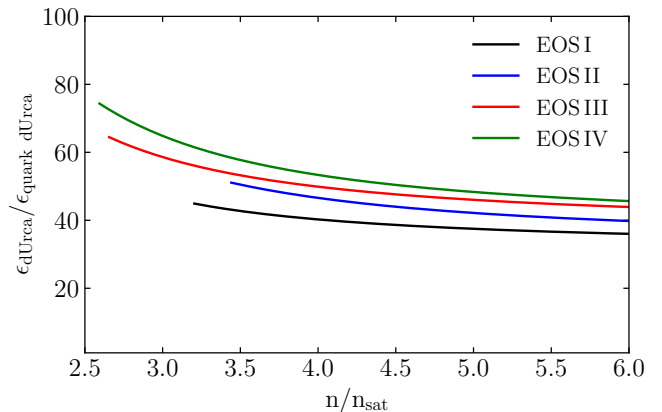


FIG. 6. Ratio of nucleonic dUrca emissivity (ϵ_{dUrca}) to quark dUrca emissivity ($\epsilon_{quark dUrca}$), assuming these reactions are simultaneously active in the quark phase, for all EOS.

cluding nuclear pairing in the nucleonic phase suppresses nucleonic dUrca reactions, turning quark dUrca into the leading cooling process. However, because the hybrid star volume in the quark phase is small, these stars often fail to reach low luminosities consistent with cold neutron stars. In this scenario, the full range of SAX J1808.4-3658's inferred luminosity has been successfully reproduced for EOS II containing weak nuclear pairing models both for protons and neutrons, and for EOS III and IV with strong proton superconductivity models. All phase transitions of EOS I are below the nucleonic dUrca threshold. This result could be an indication that twin stars with low L nucleonic EOSs, with transition density to the quark phase $4 n_{sat} \leq n_{trans}$, favor weak nuclear pairing whereas large L ones, which can only hold transition densities of $2.5 n_{sat} < n_{trans}$, favor strong proton pairing and very weak neutron triplet pairing in the nucleonic phase.

Hybrid stars that are not twin stars allow for more phase transitions, particularly above $2 n_{sat}$, consistent with astrophysical constraints, including cooling data. Thus, while twin stars can still describe observations within a certain range of phase transition densities for some EOS, this could be an indication that cooling data favours non-twin star solutions. Overall, nucleonic EOS with lower values of the slope of symmetry density L tend to allow for twin stars with larger quark-hadron phase transition densities. Furthermore, their hybrid stars tend to have lower radii, so they more easily match NICER constraints than their large L counterparts. Therefore, it is more likely for EOSs with small values of L to feature twin stars which respect astrophysical constraints, including cooling.

The cooling calculations of the quark phase have been performed with an estimate of the electron fraction of $Y_e = 10^{-5}$, and strong coupling constant, $\alpha = 0.12$. These factors determine the difference in effectiveness

of nucleonic and quark dUrca emissivities. Their ratio, which is independent of the source’s temperature, is shown in Figure 6 for all EOS studied in this work. Nucleonic dUrca reactions are just under 100 times more effective than quark dUrca reactions for these values of Y_e and α , a ratio very similar to all EOS, peaking at low densities. Therefore, when both processes are active, quark dUrca cooling is subdominant and hardly noticeable. Our estimate for the electron fraction of the quark phase was based on the assumption that it consists of up, down and strange quarks in weak equilibrium. Then, assuming the quark phase is charge neutral and that up and down quarks are approximately massless and non-interacting, one finds that $Y_e \approx 10^{-5} - 10^{-7}$ for typical quark chemical potentials of $\mu_q = 300 - 500$ MeV. This estimate is consistent with the calculations of more realistic NJL quark EOS. NJL models without color superconductivity estimate that the electron fraction for two or three flavour quark matter is, at most, of the order of $Y_e \approx 10^{-3}$, reducing with increasing density [96]. Performing the cooling calculations with this value of electron fraction for the quark phase, we obtain qualitatively similar results to the $Y_e = 10^{-5}$ case discussed in this paper: low density phase transitions for all EOS struggle to reproduce the full range of cold neutron stars’ luminosities. Furthermore, the calculated masses in the $Y_e = 10^{-3}$ scenario are smaller and the mass ranges reduced, as expected from a more efficient quark cooling.

Future work will study the effects of consistently calculated neutrino emissivities for a specific quark EOS, including color superconductivity phases, to investigate the sensitivity of these results.

ACKNOWLEDGMENTS

The authors thank Charles Gale and Andrew Cumming for insightful discussions. MM and JEC especially thank the late Stephan Wüst for suggestions and comments and dedicate this work to his memory.

MM was supported by the MITACS Globalink Research Award IT32929, the Schlumberger Foundation with a Faculty for the Future Fellowship, the European Research Council (ERC) under the European Union’s Horizon 2020 research and innovation programme (Grant Agreement No. 101020842), and by the Deutsche Forschungsgemeinschaft (DFG, German Research Foundation)—Project-ID 279384907—SFB 1245. JEC was funded by the European Research Council (ERC) Advanced Grant INSPIRATION under the European Union’s Horizon 2020 research and innovation programme (Grant agreement No. 101053985). JSB acknowledges support by the Deutsche Forschungsgemeinschaft (DFG, German Research Foundation) through the CRC-TR 211 ‘Strong-interaction matter under extreme conditions’—project number 315477589 – TRR 211.

-
- [1] D. Adhikari *et al.* (PREX), Phys. Rev. Lett. **126**, 172502 (2021), arXiv:2102.10767 [nucl-ex].
 - [2] D. Adhikari *et al.* (CREX), Phys. Rev. Lett. **129**, 042501 (2022), arXiv:2205.11593 [nucl-ex].
 - [3] Z. Zhang and L.-W. Chen, Phys. Rev. C **108**, 024317 (2023), arXiv:2207.03328 [nucl-th].
 - [4] J. M. Lattimer, Particles **6**, 30 (2023), arXiv:2301.03666 [nucl-th].
 - [5] M. H. Johnson and E. Teller, Phys. Rev. **98**, 783 (1955).
 - [6] H.-P. Duerr, Phys. Rev. **103**, 469 (1956).
 - [7] J. D. Walecka, AP **83**, 491 (1974).
 - [8] J. Boguta and A. R. Bodmer, Nucl. Phys. A **292**, 413 (1977).
 - [9] B. D. Serot and J. D. Walecka, Adv. Nucl. Phys. **16**, 1 (1986).
 - [10] H. Mueller and B. D. Serot, Nucl. Phys. A **606**, 508 (1996), arXiv:nucl-th/9603037 [nucl-th].
 - [11] B. G. Todd-Rutel and J. Piekarewicz, Phys. Rev. Lett. **95**, 122501 (2005).
 - [12] W.-C. Chen and J. Piekarewicz, Phys. Rev. C **90**, 044305 (2014).
 - [13] F. J. Fattoyev, J. Piekarewicz, and C. J. Horowitz, Phys. Rev. Lett. **120**, 172702 (2018), arXiv:1711.06615 [nucl-th].
 - [14] P. Danielewicz, R. Lacey, and W. G. Lynch, Science **298**, 1592 (2002), arXiv:nucl-th/0208016.
 - [15] A. Le Fèvre, Y. Leifels, W. Reisdorf, J. Aichelin, and C. Hartnack, Nucl. Phys. A **945**, 112 (2016), arXiv:1501.05246 [nucl-ex].
 - [16] P. Morfouace *et al.*, Phys. Lett. B **799**, 135045 (2019), arXiv:1904.12471 [nucl-ex].
 - [17] P. Demorest, T. Pennucci, S. Ransom, M. Roberts, and J. Hessels, Nature **467**, 1081 (2010), arXiv:1010.5788 [astro-ph.HE].
 - [18] J. Antoniadis, P. C. Freire, N. Wex, T. M. Tauris, R. S. Lynch, M. H. van Kerkwijk, M. Kramer, C. Bassa, V. S. Dhillon, T. Driebe, J. W. T. Hessels, V. M. Kaspi, V. I. Kondratiev, N. Langer, T. R. Marsh, M. A. McLaughlin, T. T. Pennucci, S. M. Ransom, I. H. Stairs, J. van Leeuwen, J. P. W. Verbiest, and D. G. Whelan, Science **340**, 6131 (2013), arXiv:1304.6875 [astro-ph.HE].
 - [19] E. Fonseca, T. T. Pennucci, J. A. Ellis, and other, Astrophys. J. **832**, 167 (2016), arXiv:1603.00545 [astro-ph.HE].
 - [20] H. T. Cromartie *et al.* (NANOGrav), Nature Astron. **4**, 72 (2019), arXiv:1904.06759 [astro-ph.HE].
 - [21] R. W. Romani, D. Kandel, A. V. Filippenko, T. G. Brink, and W. Zheng, Astrophys. J. Lett. **934**, L18 (2022), arXiv:2207.05124 [astro-ph.HE].
 - [22] B. P. Abbott, R. Abbott, T. D. Abbott, F. Acernese, K. Ackley, C. Adams, T. Adams, P. Addesso, R. X. Adhikari, V. B. Adya, C. Affeldt, M. Afrough, B. Agarwal, M. Agathos, K. Agatsuma, N. Aggarwal, O. D. Aguiar, L. Aiello, A. Ain, P. Ajith, B. Allen, G. Allen, A. Allocca, P. A. Altin, A. Amato, A. Ananyeva, S. B. Anderson, W. G. Anderson, S. V. Angelova, S. Antier, S. Appert, K. Arai, M. C. Araya, J. S. Areeda, N. Arnaud, K. G. Arun, S. Ascenzi, G. Ashton, M. Ast, S. M. As-

- ton, P. Astone, D. V. Atallah, P. Aufmuth, C. Aulbert, K. AultONeal, C. Austin, A. Avila-Alvarez, S. Babak, P. Bacon, M. K. M. Bader, S. Bae, M. Bailes, P. T. Baker, F. Baldaccini, G. Ballardini, S. W. Ballmer, S. Banagiri, J. C. Barayoga, S. E. Barclay, B. C. Barish, D. Barker, and et al (LIGO Scientific Collaboration and Virgo Collaboration), *Phys. Rev. Lett.* **119**, 161101 (2017).
- [23] B. P. Abbott, R. Abbott, T. D. Abbott, F. Acernese, K. Ackley, C. Adams, T. Adams, P. Addesso, R. X. Adhikari, V. B. Adya, and et al (LIGO Scientific Collaboration and Virgo Collaboration), *Phys. Rev. X* **9**, 011001 (2019).
- [24] T. E. Riley *et al.*, *Astrophys. J. Lett.* **887**, L21 (2019), arXiv:1912.05702 [astro-ph.HE].
- [25] M. C. Miller *et al.*, *Astrophys. J. Lett.* **887**, L24 (2019), arXiv:1912.05705 [astro-ph.HE].
- [26] T. E. Riley *et al.*, *Astrophys. J. Lett.* **918**, L27 (2021), arXiv:2105.06980 [astro-ph.HE].
- [27] M. C. Miller, F. K. Lamb, A. J. Dittmann, S. Bogdanov, Z. Arzoumanian, K. C. Gendreau, S. Guillot, W. C. G. Ho, J. M. Lattimer, M. Loewenstein, S. M. Morsink, P. S. Ray, M. T. Wolff, C. L. Baker, T. Cazeau, S. Manthripragada, C. B. Markwardt, T. Okajima, S. Pollard, I. Cognard, H. T. Cromartie, E. Fonseca, L. Guillemot, M. Kerr, A. Parthasarathy, T. T. Pennucci, S. Ransom, and I. Stairs, *The Astrophysical Journal* **918**, L28 (2021), arXiv:2105.06979 [astro-ph.HE].
- [28] N. Rutherford *et al.*, Accepted at *Astrophysical Journal Letters* (2024), 10.3847/2041-8213/ad5f02, arXiv:2407.06790 [astro-ph.HE].
- [29] G. Raaijmakers *et al.*, *Astrophys. J. Lett.* **887**, L22 (2019), arXiv:1912.05703 [astro-ph.HE].
- [30] G. Raaijmakers *et al.*, *Astrophys. J. Lett.* **893**, L21 (2020), arXiv:1912.11031 [astro-ph.HE].
- [31] G. Raaijmakers, S. K. Greif, K. Hebeler, T. Hinderer, S. Nissanke, A. Schwenk, T. E. Riley, A. L. Watts, J. M. Lattimer, and W. C. G. Ho, *Astrophys. J. Lett.* **918**, L29 (2021), arXiv:2105.06981 [astro-ph.HE].
- [32] V. Paschalidis, K. Yagi, D. Alvarez-Castillo, D. B. Blaschke, and A. Sedrakian, *Phys. Rev.* **D97**, 084038 (2018), arXiv:1712.00451 [astro-ph.HE].
- [33] J.-E. Christian, A. Zacchi, and J. Schaffner-Bielich, *Phys. Rev.* **D99**, 023009 (2019), arXiv:1809.03333 [astro-ph.HE].
- [34] G. Montana, L. Tolos, M. Hanauske, and L. Rezzolla, *Phys. Rev. D* **99**, 103009 (2019), arXiv:1811.10929 [astro-ph.HE].
- [35] M. Sieniawska, W. Turczanski, M. Bejger, and J. L. Zdunik, *Astron. Astrophys.* **622**, A174 (2019), arXiv:1807.11581 [astro-ph.HE].
- [36] J.-E. Christian and J. Schaffner-Bielich, *Astrophys. J. Lett.* **894**, L8 (2020), arXiv:1912.09809 [astro-ph.HE].
- [37] D. D. Ivanenko and D. F. Kurdgelaidze, *Astrophys. J.* **1**, 251 (1965).
- [38] N. Itoh, *Prog.Theor.Phys.* **44**, 291 (1970).
- [39] M. Alford, M. Braby, M. Paris, and S. Reddy, *Astrophys.J.* **629**, 969 (2005), arXiv:nucl-th/0411016 [nucl-th].
- [40] J. Coelho, C. Lenzi, M. Malheiro, J. Marinho, R.M., and M. Fiolhais, *Int.J.Mod.Phys.* **D19**, 1521 (2010), arXiv:1001.1661 [nucl-th].
- [41] H. Chen, M. Baldo, G. Burgio, and H.-J. Schulze, *Phys.Rev.* **D84**, 105023 (2011), arXiv:1107.2497 [nucl-th].
- [42] K. Masuda, T. Hatsuda, and T. Takatsuka, *Astrophys. J.* **764**, 12 (2013), arXiv:1205.3621 [nucl-th].
- [43] N. Yasutake, R. Lastowiecki, S. Benic, D. Blaschke, T. Maruyama, and T. Tatsumi, *Phys.Rev.* **C89**, 065803 (2014), arXiv:1403.7492 [astro-ph.HE].
- [44] A. Zacchi, M. Hanauske, and J. Schaffner-Bielich, *Phys. Rev.* **D93**, 065011 (2016), arXiv:1510.00180 [nucl-th].
- [45] B. Kämpfer, *J.Phys.* **A14**, L471 (1981).
- [46] N. K. Glendenning and C. Kettner, *AA* **353**, L9 (2000), astro-ph/9807155.
- [47] K. Schertler, C. Greiner, J. Schaffner-Bielich, and M. H. Thoma, *NP* **A677**, 463 (2000), astro-ph/0001467.
- [48] J. Schaffner-Bielich, M. Hanauske, H. Stöcker, and W. Greiner, *Physical Review Letters* **89**, 171101 (2002), astro-ph/0005490.
- [49] J. Zdunik and P. Haensel, *Astron.Astrophys.* **551**, A61 (2013), arXiv:1211.1231 [astro-ph.SR].
- [50] M. G. Alford, G. Burgio, S. Han, G. Taranto, and D. Zappalà, *Phys. Rev.* **D92**, 083002 (2015), arXiv:1501.07902 [nucl-th].
- [51] D. Blaschke and D. E. Alvarez-Castillo, *Proceedings, 11th Conference on Quark Confinement and the Hadron Spectrum (Confinement XI): St. Petersburg, Russia, September 8-12, 2014*, AIP Conf. Proc. **1701**, 020013 (2016), arXiv:1503.03834 [astro-ph.HE].
- [52] M. G. Alford and A. Sedrakian, *Phys. Rev. Lett.* **119**, 161104 (2017), arXiv:1706.01592 [astro-ph.HE].
- [53] J.-E. Christian, A. Zacchi, and J. Schaffner-Bielich, *Eur. Phys. J.* **A54**, 28 (2018), arXiv:1707.07524 [astro-ph.HE].
- [54] S. M. de Carvalho, R. Negreiros, M. Orsaria, G. A. Contrera, F. Weber, and W. Spinella, *Phys. Rev. C* **92**, 035810 (2015).
- [55] F. Lyra, L. Moreira, R. Negreiros, R. O. Gomes, and V. Dexheimer, *Phys. Rev. C* **107**, 025806 (2023), arXiv:2206.01679 [astro-ph.HE].
- [56] M. Mendes, F. J. Fattoyev, A. Cumming, and C. Gale, *The Astrophysical Journal* **938**, 119 (2022).
- [57] A. Y. Potekhin, M. E. Gusakov, and A. I. Chugunov, “Thermal evolution of neutron stars in soft x-ray transients with thermodynamically consistent models of the accreted crust,” Pre-print (2023), arXiv:2303.08716 [astro-ph.HE].
- [58] F. Fattoyev, *Sensitivity of neutron star properties to the equation of state*, phdthesis, The Florida State University (2011).
- [59] B. T. Reed, F. J. Fattoyev, C. J. Horowitz, and J. Piekarewicz, *Phys. Rev. C* **109**, 035803 (2024), arXiv:2305.19376 [nucl-th].
- [60] Z. Zhang and L.-W. Chen, *Phys. Rev. C* **90**, 064317 (2014), arXiv:1407.8054 [nucl-th].
- [61] B. T. Reed, F. J. Fattoyev, C. J. Horowitz, and J. Piekarewicz, *Phys. Rev. Lett.* **126**, 172503 (2021), arXiv:2101.03193 [nucl-th].
- [62] B.-J. Cai and L.-W. Chen, *Nucl. Sci. Tech.* **28**, 185 (2017), arXiv:1402.4242 [nucl-th].
- [63] M. Rufa, P. G. Reinhard, J. A. Maruhn, W. Greiner, and M. R. Strayer, *Phys. Rev. C* **38**, 390 (1988).
- [64] F. J. Fattoyev, J. Carvajal, W. G. Newton, and B.-A. Li, *Phys. Rev. C* **87**, 015806 (2013), arXiv:1210.3402 [nucl-th].
- [65] S. Ghosh, B. K. Pradhan, D. Chatterjee, and J. Schaffner-Bielich, *Front. Astron. Space Sci.* **9**, 864294 (2022), arXiv:2203.03156 [astro-ph.HE].
- [66] J. M. Lattimer and A. W. Steiner, *Eur. Phys. J. A* **50**, 40 (2014), arXiv:1403.1186 [nucl-th].

- [67] M. Mendes, A. Cumming, C. Gale, and F. J. Fattoyev, in *16th Marcel Grossmann Meeting on Recent Developments in Theoretical and Experimental General Relativity, Astrophysics and Relativistic Field Theories* (2021) arXiv:2110.11077 [nucl-th].
- [68] M. G. Alford, S. Han, and M. Prakash, *Phys. Rev. D* **88**, 083013 (2013).
- [69] J.-E. Christian, J. Schaffner-Bielich, and S. Rosswog, *Phys. Rev. D* **109**, 063035 (2024), arXiv:2312.10148 [nucl-th].
- [70] G. Baym, C. Pethick, and P. Sutherland, *Astrophys. J.* **170**, 299 (1971).
- [71] J. Negele and D. Vautherin, *Nucl. Phys. A* **207**, 298 (1973).
- [72] J. Piekarewicz, F. J. Fattoyev, and C. J. Horowitz, *Phys. Rev. C* **90**, 015803 (2014).
- [73] Z. F. Seidov, *Soviet Astronomy* **15**, 347 (1971).
- [74] M. Alford, private communication (2024).
- [75] D. Yakovlev, A. Kaminker, O. Gnedin, and P. Haensel, *Physics Reports* **354**, 1 (2001).
- [76] N. Iwamoto, *Phys. Rev. Lett.* **44**, 1637 (1980).
- [77] G. W. Carter and M. Prakash, *Physics Letters B* **525**, 249 (2002).
- [78] W. C. G. Ho, K. G. Elshamouty, C. O. Heinke, and A. Y. Potekhin, *Phys. Rev. C* **91**, 015806 (2015).
- [79] P. S. Shternin, D. G. Yakovlev, C. O. Heinke, W. C. G. Ho, and D. J. Patnaude, *Monthly Notices of the Royal Astronomical Society: Letters* **412**, L108 (2011), <https://academic.oup.com/mnrasl/article-pdf/412/1/L108/3262203/412-1-L108.pdf>.
- [80] L. Amundsen and E. Østgaard, *Nuclear Physics A* **442**, 163 (1985).
- [81] O. Elgarøy, L. Engvik, M. Hjorth-Jensen, and E. Osnes, *Nuclear Physics A* **607**, 425 (1996).
- [82] J. Chen, J. Clark, R. Davé, and V. Khodel, *Nuclear Physics A* **555**, 59 (1993).
- [83] M. Baldo, J. Cugnon, A. Lejeune, and U. Lombardo, *Nuclear Physics A* **536**, 349 (1992).
- [84] E. F. Brown, A. Cumming, F. J. Fattoyev, C. Horowitz, D. Page, and S. Reddy, *Physical Review Letters* **120** (2018), 10.1103/physrevlett.120.182701.
- [85] A. Cumming, E. F. Brown, F. J. Fattoyev, C. J. Horowitz, D. Page, and S. Reddy, *Phys. Rev. C* **95**, 025806 (2017).
- [86] A. S. Parikh, R. Wijnands, L. S. Ootes, D. Page, N. Degenaar, A. Bahramian, E. F. Brown, E. M. Cackett, A. Cumming, C. Heinke, J. Homan, A. Rouco Escorial, and M. J. P. Wijngaarden, *Astronomy & Astrophysics* **624**, A84 (2019), arXiv:1810.05626 [astro-ph.HE].
- [87] A. Cumming, E. F. Brown, F. J. Fattoyev, C. J. Horowitz, D. Page, and S. Reddy, *Phys. Rev. C* **95**, 025806 (2017), arXiv:1608.07532 [astro-ph.HE].
- [88] Potekhin, A. Y., Chugunov, A. I., and Chabrier, G., *A&A* **629**, A88 (2019).
- [89] C. O. Heinke, P. G. Jonker, R. Wijnands, C. J. Deloye, and R. E. Taam, *The Astrophysical Journal* **691**, 1035 (2009).
- [90] A. Burrows, D. Radice, D. Vartanyan, H. Nagakura, M. A. Skinner, and J. C. Dolence, *Monthly Notices of the Royal Astronomical Society* **491**, 2715 (2019), <https://academic.oup.com/mnras/article-pdf/491/2/2715/31221715/stz3223.pdf>.
- [91] Y. Suwa, T. Yoshida, M. Shibata, H. Umeda, and K. Takahashi, *Monthly Notices of the Royal Astronomical Society* **481**, 3305 (2018), <https://academic.oup.com/mnras/article-pdf/481/3/3305/25834769/sty2460.pdf>.
- [92] D. Radice, A. Burrows, D. Vartanyan, M. A. Skinner, and J. C. Dolence, *Astrophys. J.* **850**, 43 (2017), arXiv:1702.03927 [astro-ph.HE].
- [93] H. T. Janka, B. Müller, F. S. Kitaura, and R. Buras, *Astronomy & Astrophysics* **485**, 199 (2008), arXiv:0712.4237 [astro-ph].
- [94] T. Fischer, S. C. Whitehouse, A. Mezzacappa, F. K. Thielemann, and M. Liebendörfer, *Astronomy & Astrophysics* **517**, A80 (2010), arXiv:0908.1871 [astro-ph.HE].
- [95] J.-E. Christian and J. Schaffner-Bielich, *Astrophys. J.* **935**, 122 (2022), arXiv:2109.04191 [astro-ph.HE].
- [96] M. Buballa, *Phys. Rept.* **407**, 205 (2005), arXiv:hep-ph/0402234.